CHAPTER 123

WAVE-FORMED RIPPLES IN NEARSHORE SANDS

John R. Dingler[1]
Douglas L. Inman[2]

ABSTRACT

Ripples are generated and modified by wind-generated waves and their profiles are controlled by the nature of the near-bottom wave motion and by the size of the bed material. Wave-formed ripples develop under a definable set of conditions called the ripple regime. The ripple regime is bounded by those conditions that initiate grain motion, low-wave intensity, and by those that cause the disappearance of ripples, onset of sheet flow. Sheet flow occurs when intense wave motion causes several grain layers to be in motion. Three distinct ripple types occur in nearshore areas of fine sand - relict ripples, vortex ripples, and transition ripples. Vortex and transition ripples lie within the active ripple regime, whereas relict ripples do not.

Ripples in fine sand were studied in the field at La Jolla, California, where profiles were obtained using a newly developed high-resolution sonar capable of vertical resolution of the order of one millimeter. Simultaneous profile and wave-pressure measurements permit correlation of the ripple profiles with individual waves and with the wave spectrum. The sonar, with its rapid scan capability ($\sim$ one meter per second), gives instantaneous measurement of the actively changing bed features in nearshore waters. The combination of bottom scans and wave-pressure measurements extends previous wave-ripple studies to include all of the nearshore ripple regime.

The relation between the wave and ripple data from this study is best shown by plotting ripple steepness η/λ against the wave form of the Shields relative stress criterion Θ. Vortex ripples ($\eta/\lambda \lesssim 0.15$) occur for Θ values less than 40 but greater than the minimum value which is determined by the onset of grain motion.

The transition from vortex ripples to sheet flow commences at a Θ value around 40 and ends at $\Theta_c \lesssim 240$, where Θ_c is the critical value for the onset of sheet flow. With transition ripples, the decrease in steepness is caused by a decrease in ripple height, since the ripple wavelength remains essentially constant. Beds that become planar as a result of intense wave conditions ($\Theta > 240$) re-ripple in a few wave cycles once the intensity decreases. For this reason, bottom scans taken before equilibrium is reestablished show ripples that have a low steepness.

---

1. U. S. Geological Survey, Menlo Park, CA 94025
2. Scripps Institution of Oceanography, La Jolla, CA 92093

During some experiments where no sheet flow occurred between scans, migration of transition ripples was measured and found to range between zero and four centimeters per minute, increasing with increasing values of the theoretical bottom wave-drift current. Whenever migration was observed, it was in the direction of wave propagation, i.e., onshore.

Ripple symmetry is the ratio of the horizontal crest-to-trough distance β (in the direction of wave travel) to the ripple wavelength λ. A β/λ value of 0.50 indicates a symmetric ripple. Measured values of β/λ ranged from 0.36 to 0.61 with 74% of the values in the range 0.45 - 0.55, and 55% in the range 0.47 - 0.53.

INTRODUCTION

When progressive surface gravity waves shoal, interactions occur between the oscillating fluid and the bottom sediment. When these interactions become sufficiently intense, ripples develop on bottoms composed of sand. The oscillatory nature of the flow produces ripples that are generally symmetric in cross section, a geometry that is discernible from the distinctly asymmetric ripples formed by unidirectional flows. If the wave conditions remain constant for a long enough period of time, the ripples reach an equilibrium state with constant values of height and wavelength. The equilibrium ripple geometry is a function of the sand size and the character of the wave action above the bottom.

As shoaling progresses the near-bottom orbital velocities become more intense. This produces a ripple regime within which ripple sizes change systematically and within which each ripple is in equilibrium with the waves over it. For time periods of the order of a wave period, the movement of a ripple is characterized by an onshore-to-offshore oscillation of the ripple crest as first the wave crest and then the wave trough pass over the ripple. Any net movement of the ripple over longer time periods is related to differences in the crest and trough orbital velocities that occur in shallow water.

Flow conditions commensurate with the ripple regime occur over much of the nearshore, and the profile of the ripples varies within this region (Figure 1). In deeper water, where the wave action is generally too weak to move the sand, the bed generally contains relict ripples which formed under earlier, more intense wave action and which are gradually reworked by organisms. Ripples form once the wave action is of sufficient strength to move sand. Although the ripple height η and wavelength λ change as the wave intensity increases, the ripple steepness η/λ remains relatively constant (vortex ripples) until the bottom is subjected to the very strong flows that normally occur in relatively shallow water. As the flow strength increases beyond the conditions where vortex ripples occur, the ripples become less steep (transition ripples) until finally the ripples disappear as several grain layers are in motion (sheet flow regime). In deeper water the ripples tend to be relatively short crested, giving the bed a three-dimentional appearance (Inman, 1957). By the time transition ripples develop, ripple crests are quite long and the bed has become markedly two-dimensional in appearance.

Previous Work

Hunt (1882) and Darwin (1883), using laboratory wave tanks, were among the first to show that symmetrical ripples could be produced by oscillatory water motions. The work of Bagnold (1946) quantified the relation between ripple size and flow conditions. Bagnold's work has been extended by subsequent investigators, and now many aspects of oscillation ripples can be predicted with some degree of accuracy.

Bagnold's classic experiments on oscillation ripples demonstrated the relation between orbital diameter and ripple wavelength when flow conditions are near the threshold of grain motion (Figure 2). Once grains begin moving, ripples form and their wavelength is approximately equal to the orbital diameter. Increases in orbital diameter cause an increase in wavelength until a limiting value is reached, and the limiting value is grain size dependent. Over the range of orbital diameters studied by Bagnold, the wavelength was not a function of the period of oscillation. Bagnold did not extend the experiments to more intense flow conditions to determine whether the wavelength remained constant until sheet flow occurred.

Inman (1957), in a comprehensive field study of wave-formed ripples, obtained the ripple wavelengths by marking with grease pencil on clear plastic laid on top of the ripples. The near-bottom orbital displacements were measured *in situ*, while the wave period was obtained from the record of a fathometer mounted on a small boat. The results of Inman's work are shown in Figure 3. Except for a few points, ripple wavelength generally decreases with increasing orbital diameter. The Inman field data was produced under larger orbital diameters than the Bagnold laboratory data. Combining the two data sets reinforces Bagnold's observation that the ripple wavelength can only increase to a certain point with increasing orbital diameter. Then, rather than remain constant, as might be inferred from Bagnold's data, the wavelength actually decreases again. These aspects of ripple wavelength are integrated into a conceptual model of sedimentary structures by Clifton (1976).

Inman's rough estimates of ripple height gave a steepness value on the order of 0.15 except in the more intense flow regimes where the steepness began to decrease. Carstens, and his coworkers (1969), looking at oscillation ripples on sand beds using a pulsating water tunnel, also observed that the ripple steepness decreased from 0.15 under the most intense flows.

Most nearshore sands are composed of material with density similar to that of quartz (density of 2.65 gm/cm^3). It is important, however, that the variation of ripple form with grain density be studied for application to heavy mineral environments and to movable bed modeling. Mogridge and Kamphuis (1972) showed that variations in ripple height and wavelength can be significant, but that the ripple steepness is only weakly affected by grain density since the height and wavelength variations tend to cancel out. They further state that the importance of grain density diminishes as the wave period increases since fluid accelerations become less important at the longer periods.

Present Study

Previous studies show that the equilibrium ripple wavelength is a function of the grain size of the sediment and of the near-bottom orbital diameter of the oscillating fluid. Some of the earlier studies also suggest that the ripple steepness decreases systematically prior to sheet flow (it is zero at the onset of sheet flow). This study, undertaken as part of a doctoral program at the Scripps Institution of Oceanography (Dingler, 1974), establishes criteria for the limits of the ripple regime and describes the ripple geometry in the transition zone between constant steepness ripples and sheet flow. The lower limit of the ripple regime (onset of grain motion) was studied in a large wind-wave channel using oceanic wave periods and heights (Dingler, 1974). The upper limit (onset of sheet flow) and the ripple profile in the transition zone were determined by field measurement using a newly developed profiler. Most of the experiments were performed in the vicinity of the Scripps pier where the sediment is a well-sorted fine quartz sand.

THEORETICAL CONSIDERATIONS

Wave Relations

The wave and ripple parameters used in this study are sketched in Figure 4. The near-bottom orbital velocity u at any point is related to the maximum velocity u_m and the phase of the wave by

$$u = u_m \cos(\sigma t)$$

where t is time, $\sigma = 2\pi/T$ is the angular frequency of oscillation and T is the wave period (linear wave theory; Airy, [1845]). The maximum velocity, which occurs during crest and trough passage, is given by

$$u_m = \frac{\pi d_o}{T} = \frac{\sigma H}{2 \sinh(kh)} \qquad (1)$$

where d_o is the orbital diameter, h is the water depth, H is the wave height, $k = 2\pi/L$ is the wave number and L is the wave length at the point of interest. The value of kh is obtained for a given depth and period by iterative solution of the wave dispersion relation

$$\left[\frac{2\pi}{T}\right]^2 \frac{h}{g} = kh \tanh(kh)$$

where g is the acceleration of gravity. In shallow water ($h/L < 1/20$) deviations from linear theory become significant with the exception that the near-bottom velocities are still reasonably predictable from linear theory (LeMehuate, et al., 1969; May, 1975).

When the wave train consists of waves of varying amplitudes and frequencies, Fourier analysis techniques are used to analyze the time series of the wave record. The technique used in this study follows the procedure of Cooley and Tukey (1965) with the final output being a plot of the mean-square elevation of the water surface $\langle \eta^2 \rangle$ per fre-

quency band Δf. Since the mean energy per unit area of water surface E is related to $\langle\eta^2\rangle$ by

$$E = \rho g\langle\eta^2\rangle = 1/8\rho g H^2_{rms}$$

where H_{rms} is the root-mean-square wave height, $\langle\eta^2\rangle$ is proportional to the available wave energy given that the fluid weight per unit volume ρg remains essentially constant for sea water. Then, u_m is related to $\langle\eta^2\rangle$ by

$$u_m = \frac{\sigma(2\langle\eta^2\rangle)^{\frac{1}{2}}}{\sinh(kh)} .$$

Another commonly used parameter, the significant wave height $H_{1/3}$, is assumed to be given by

$$H_{1/3} = \sqrt{2}\ H_{rms} .$$

Dimensional Analysis

The ripple steepness η/λ is a function of seven independent variables. These seven variables are (1) fluid related: the fluid viscosity μ and density ρ; (2) sediment related: the grain density ρ_s and grain size D; and (3) flow related: the near-bottom orbital diameter d_o, the period of oscillation T, and the acceleration due to gravity g (note that grain-shape factors are not included in this analysis, although a completely general analysis would include shape and packing). Since u_m, d_o and T are related in linear theory (Equation 1), only two of these three variables are required to specify the wave conditions. As the immersed weight of the sediment depends on a density difference, the factor converting volume to immersed weight γ_s,

$$\gamma_s = (\rho_s - \rho)g$$

replaces gravity as an independent variable. The complete dimensional functional relation is given by

$$\eta/\lambda = f(\rho, \mu, \rho_s, D, d_o, T, \gamma_s)$$

and this is non-dimensionalized to give the functional relation

$$\eta/\lambda = \Phi\left[\frac{\rho\gamma_s D^3}{\mu^2}, \frac{\gamma_s T^2}{\rho D}, \frac{d_o}{D}, \frac{\rho_s}{\rho}\right] . \qquad (2)$$

Equation (2) will be represented in shorthand notation by

$$\eta/\lambda = \Phi\ (X_1, X_2, X_3, X_4) .$$

A fifth dimensionless variable, the wave form of the Shields relative stress criterion Θ, is obtained by combining X_2 and X_3.

$$\Theta = \pi^2 X_3^2 / X_2 = \rho u_m^2 / \gamma_s D.$$

The dimensionless variable X_1 is equal to Re^2/Θ, where $Re = \rho u_m D/\mu$ is a Reynolds number. Although Re and Θ include flow parameters, X_1 is formed by the fluid and granular properties only. It therefore reflects the influence of viscosity independent of the stage of the fluid-granular motion, and remains constant throughout the stages of the flow. The dimensionless variable X_2 indicates the influence of wave period. The dimensionless variable X_3 indicates the importance of the drag force F_D to the inertial force F_I in an oscillatory system. Thus,

$$F_D \sim D^2 u^2$$

and

$$F_I \sim D^3 (du/dt).$$

For oscillatory flow

$$du/dt = u_m \sigma \sin(kx - \sigma t).$$

Then

$$\frac{F_D}{F_I} \sim \frac{D^2 [u_m \cos(kx - \sigma t)]^2}{D^3 u_m \sigma \sin(kx - \sigma t)}.$$

Comparing maximum values, even though they are 90° out of phase, yields

$$\frac{F_D}{F_I} \sim \frac{u_m}{D} = \frac{d_o}{2D} = \frac{X_3}{2}.$$

The dimensionless variable X_4 is the "specific mass" and indicates the influence of the mass of grains ρ_s relative to that of fluid ρ. Since ρ_s is associated with inertial forces of the grains, its nondimensional form X_4 may be significant whenever grains are subjected to nongravitational accelerations.

EXPERIMENTAL PROCEDURE AND DATA ANALYSIS

The results of this study are based primarily on field data as bed forms in the large wind-wave channel at Scripps were influenced by the channel boundaries during intense flow conditions. Most of the study was conducted in the high-energy nearshore environment at La Jolla, California, where flow conditions were sufficient to produce both ripples and a flat bed (Figure 5).

Ripple Profiling

Oscillation ripples on beds of fine sand tend to have elevations of the order of a centimeter and lengths of the order of a decimeter.

Ripple wavelengths can be measured rather accurately in situ with a meter stick, but ripple heights are almost impossible to measure manually because the weight of the meter stick flattens the crests and because constant water motion from the waves disrupts the measurement. To overcome this difficulty, a sediment surface profiler using high frequency sound waves (4.5 MHz) was developed (Dingler, et al., unpublished manuscript). The vertical resolution of the sonar was ascertained to be at least 1 mm. The sonar head was mounted in an open aluminum framework that sat about 25 cm above the bottom (Figure 6). The frame was easily transported and relatively scour free. Visual observations during field experiments under various flow conditions indicated that the flow disturbance caused by the sonar frame did not reach the sand bed.

Procedure

Most of the experiments were undertaken in the vicinity of the Scripps pier. Two Scuba divers entered the water at the end of the pier and the sonar frame with attached pressure sensor was lowered to the divers. The divers carried the sonar away from the pier in order to eliminate effects of the pier on the flow field and oriented the frame on the bottom normal to the ripple crests (Figure 6). A surface sample of sand was collected from each site.

Each experiment lasted at least 8.5 minutes. The procedure was repeated as many as three times at stations spaced about 70 m apart (on-offshore). Often wave intensities were such that sheet-flow conditions extended far enough offshore to permit only one experiment.

Sonar scans occurred about once a minute and each scan required from three to six seconds to complete. Generally, the scans were made to coincide with lulls in wave activity in order to minimize profile errors caused by crest movement during the passage of moderate to large waves. Also, under intense flow conditions, there was sufficient sand in suspension just above the bottom that the sonar responded to the suspended load rather than to the bed forms.

Data Reduction and Analysis

All the data was cabled to a shelf station where it was transmitted to the laboratory via the Shore Process Laboratory SAS system (Lowe, et al., 1972). The data was first digitized at a sample rate of 125 times per second with a 10 bit resolution. Then it was recorded on both strip chart and on magnetic tape. Each ripple profile was plotted from tape on graph paper and the data on the plots reduced by hand. Averages and standard deviations were obtained for ripple height, wavelength and asymmetry, and the averages were used in subsequent calculations. Finally, by following individual ripple crests from profile to profile an estimate of the migration rate for the ripples was obtained.

In some experiments the bed was smoothed by intense flows and subsequently re-rippled. In these cases the use of spectral wave parameters would be inappropriate. Instead, the analog pressure record was

directly analyzed and the wave parameters calculated from a few large waves that occurred before the scan of interest.

RESULTS AND DISCUSSION

Oscillation ripples occur over a range of definable flow conditions. The lower limit is the onset of grain motion and the upper limit is the occurrence of sheet flow. Within these limits the ripples have a cross-sectional geometry that is predictable when the flow intensity and grain size are known. Based on steepness, two types of ripples are found: vortex ripples (ripple steepness $\sim$ o.15) and transition ripples (ripple steepness $<$ 0.15).

Ripple Geometry

Two data reduction procedures were used on the wave data in this study. In the first procedure the flow parameters were calculated from the wave spectrum and represent the root-mean-square values as recorded over an interval of 8.5 minutes. In the second procedure the near-bottom flow parameters were calculated from a short section of the wave record preceding the sonar scan and represent the "instantaneous" conditions prior to the measurement. In subsequent discussions the latter procedure will be referred to as the "single wave" procedure. It was employed only when flat bed conditions had been observed at some time during the experiment.

The nature of field experimentation generally precludes systematic variation of one dimensionless variable while holding the others constant as can be done in the laboratory. In the dimensionless functional relation

$$\eta/\lambda = \Phi(X_1, X_2, X_3, X_4)$$

the dimensionless variables X_1 and X_4 are independent of the flow conditions. By selecting field locations where the sediment is material of quartz density and where the grain-size variations are small, the effect of the variables X_2 and X_3 can be analyzed independent of X_1 and X_4. When the data for fine sand is plotted as

$$\eta/\lambda = \Phi_1(X_2^a X_3^b)$$

on log-log paper, values of a = -1, b = 2 produce a coherent trend to the data. This is not surprising as this combination of the two dimensionless groups is proportional to the relative stress Θ (Equation 3) which is an important variable in many fluid-granular interactions.

Ripple steepness is plotted as a function of relative stress in Figure 7. Although the data shows a consistent trend when plotted in this manner, the steepness values begin to decrease at a lower value of the relative stress than in the studies of Inman and Carstens, et al. This occurs because there is a fundamental difference in analysis procedures. Bed forms for fine sand respond rapidly (i.e., in one or two wave periods) to changes in wave characteristics. The "single wave" procedure, which emphasizes instantaneous conditions, is thus similar to

the constant wave conditions of the laboratory. The spectral analysis procedure, on the other hand, considers waves of varying height and period occurring over a time period of 8.5 minutes. To emphasize the importance of larger waves on the ripple geometry, Inman used an orbital diameter parameter based on the significant wave rather than the root-mean-square wave. When Figure 7 is modified to emphasize the importance of the larger waves on the ripples (Figure 8), correlation is significantly improved for those conditions where the data sets overlap.

Figure 9 is a five minute record of the second experiment of 26 October 1972 at a water depth of 3.4 meters. The top trace is the wave record as measured at the pressure sensor. The second trace shows the output of the sonar head as it sat at the onshore end of the track. The third trace gives time relative to the start of the experiment. The times of the scans are indicated by arrows and the scans are shown in the bottom four traces. At the time of scan 1 the bed was rippled and the steepness value fell on the equilibrium curve of Figure 8. Subsequently, a set of large waves produced sheet flow and a flat bed (scan 2). Following the passage of several smaller waves the bed again was rippled, although the steepness had not yet reached an equilbrium value (scan 3). Before equilibrium was reached a set of two large waves almost re-leveled the bed (scan 4). This series of bed profiles shows that in fine sand the bed responds rapidly to intense flow and a bed can be flattened and re-rippled in a time equivalent to a few wave periods.

The transformation of a fine sand bottom from transition ripples to a flat bed occurs over one or two wave periods. Assume that the bottom is subjected to waves of variable height and of sufficient intensity that transition ripples occur following the passage of intermediate height waves, while the largest waves produce sheet flow and a flat bottom. Once the flat bottom occurs, it persists during periods of the smallest waves because they are not of sufficient intensity to move the sand. As the wave conditions intensify, sediment begins to move and vortex ripples start to form. If these wave conditions were to persist for a sufficient time (minutes), the ripples would eventually reach an equilibrium configuration with a steepness of about 0.15. This wave pattern does not persist for more than a few wave cycles in such a variable system and only transition ripples form.

Transition ripples occur for relative stresses greater than 40, but less than the critical value for sheet flow. The decrease in steepness of the transition ripples is attributable to decrease in ripple height since the experiments show that the ripple wavelength itself remains constant for these flow conditions (Figure 10). At a critical relative stress value of 240 sheet flow prevails and a flat bed again forms. The growth of the ripples from a flat bed to transition ripples is schematized by dashed lines in Figure 8.

The effect on ripple steepness of the dimensionless variable $X_1 = \rho\gamma_s D^3/\mu^2$ was not determined conclusively because of a lack of good study sites with coarse sand. The only usable information on the importance of larger grain sizes came from some preliminary laboratory experiments and from a few field experiments. All of the laboratory and all

but two of the field data points were for vortex ripples (Figures 7 and 8). The two transition ripple values fall with the fine sand values, which suggests that ripple steepness does not strongly depend on the dimensionless variable X_1. This is consistent with the findings of Mogridge and Kamphuis (1973).

Because the grain density remained constant for the field experiments, X_4 was not evaluated. Mogridge and Kamphuis state that this variable is not important with respect to the ripple steepness although X_4 does have a significant effect on the ripple height and wavelength.

The criterion for the onset of grain motion under progressive waves has been shown to be

$$\frac{\gamma_s T^2}{\rho D} = 240 \left[\frac{do}{D}\right]^{\frac{4}{3}} \left[\frac{\rho \gamma_s D^3}{\mu^2}\right]^{-\frac{1}{9}}$$

when the grain diameter is less than the (theoretical) thickness of the wave-formed boundary layer (Dingler, 1974). Rearrangement of this relationship in terms of the threshold relative stress θ_t gives

$$\theta_t = 0.0027 \ (\gamma_s^2/\rho\mu)^{\frac{1}{3}} \ T. \qquad (4)$$

For the case of material of quartz density (ρ_s = 2.65 gm/cm^3) in a typical nearshore environment (ρ = 1.0 gm/cm^3, μ = 1.1 centipoise), equation (4) reduces to

$$\theta_t = (1.7 \text{ sec}^{-1}) \ T.$$

In Figure 8 this relation has been superimposed upon the curve for the equilibrium ripple steepness to indicate the lower limit of the ripple regime for various wave periods.

Ripple Migration

Ripple migration under oscillatory flow conditions might be expected to occur when a net fluid flow is superimposed on the oscillations. The bottom wave-drift current has been shown to produce an onshore ripple migration in the laboratory (Inman and Bowen, 1963). Ripple migration is a critical aspect of sediment transport over the shelf since the rate of grain migration is inherently related to the burial and exposure of the grains by the moving ripple form (Inman and Bagnold, 1963). Study of ripple migration for transition ripples is complicated by the occasional destruction or near destruction of the ripples and by the associated high sediment concentrations in sheet flow. The migration rate of the sand thus involves both movement of the ripple form and movement by sheet flow.

The intermittent scanning of the bottom prevented ripple migration measurements for every experiment. Yet in several experiments, the position of individual ripple crests could be traced from scan to scan and the migration rates of these ripples showed a positive correlation

with the theoretical bottom wave-drift current u_Θ (Table 1).

$$u_\Theta = 5/4\ u_m^2\ T/L. \quad (5)$$

A better understanding of the nature of the bottom wave-drift current over rippled beds is necessary before a more detailed study of ripple migration rates can be attempted.

Table 1

Ripple migration rates obtained from repeated sonar scans. The bottom wave-drift current u_Θ is calculated from Equation 5 using rms values from the wave spectral analysis.

Experiment	u_Θ, cm/sec	Migration rate cm/min
1	4.7	4.2
6	3.2	1.2
11	2.8	0.5
9	1.2	0.0

Ripple Shape and Variability

Analysis of the ripple profiles included the measurement of the horizontal distance from crest to onshore trough β, which when divided by the wavelength λ, is indicative of the symmetry of the ripple form. The ripple symmetry factor β/λ is 0.50 for a symmetrical ripple, less than 0.50 when the ripple has a steep onshore facing crest, and greater than 0.50 for a steep offshore facing crest. The measured values of β/λ ranged from 0.36 to 0.61 with 74% of the values in the range 0.45 - 0.55, and 55% in the range 0.47 - 0.53. There was no correlation between the symmetry value and the relative stress for the spectrally related ripples, but this can be attributed to the fact that the ripple scans followed specific waves while the relative stress was based on 8.5 minutes of wave record. Even though the ripple height and length do not change with every wave for non-sheet flow conditions, a large wave crest or trough could slightly modify the steepness factor by a slight onshore or offshore movement of the ripple crest. Some uncertainty in the measurement of β due to the flat nature of ripple troughs also contributed to the range of symmetry values. The β/λ values for the "single wave" ripples showed some correlation with the relative stress such that a β/λ value of 0.42 corresponded to the lowest relative stress value and β/λ increased to 0.48 with increasing relative stress.

Standard deviations were calculated for the ripple parameters η, β, and λ. For comparative purposes these values were expressed as the coefficient of variation that is defined as the ratio of the standard deviation to the mean value. For all the data, the values of the coefficient of variation for η and β were generally between 0.10 and 0.25 while for λ they were often less than 0.10. Some of the variation in the ripple elevation is probably due to the fact that the elevations were generally so small that their measurement has a lower relative accuracy than that of the other parameters. The β measurements were

more variable than the λ measurements because of the greater difficulty in determining the exact location of the lowest part of the trough.

CONCLUSIONS

From this study of wave-formed ripples in a high-energy nearshore sand environment these conclusions are drawn:

1. Once ripples form, their steepness is controlled by the relative stress. The steepness remains constant until the relative stress reaches a value of 40, then decreases to zero (flat bed) for sheet flow.

2. Sheet flow, which produces flat beds, commences at a value of the relative stress of 240.

3. Relative stresses greater than 240 cause ripples in fine sand to disappear and the bed to become flat after the passage of one or two large waves. A rippled bed reappears after the passage of a few smaller waves.

4. Ripple migration rates in fine sand range from zero to 4.2 cm per minute. The migration is always onshore and can be correlated with the theoretical bottom wave-drift current.

5. Grain size appears to have negligible effect on steepness of vortex or transition ripples. It should be noted however, that the maximum ripple wavelength and height are grain size dependent.

6. Ripple symmetry ranged from 0.36 to 0.61 with 55% of the values falling in the range 0.47 - 0.53 and 74% in the range 0.45 - 0.55.

7. A sonic bed profiler operating at 4.5 MHz is capable of resolving the ripple elevation to at least 1 mm and works well in both the laboratory and the field.

Acknowledgements

This research was supported by the Sea Grant Program and the Office of Naval Research under contract with the Scripps Institution of Oceanography, University of California, La Jolla, California.

REFERENCES

Airy, G. B., 1845, "On tides and waves", Encyclopedia Metropolitana, vol. 5, p. 241-396.

Bagnold, R. A., 1946, "Motion of waves in shallow water; interaction between waves and sand bottoms", Proc. Roy. Soc. London A, 187, p. 1-15. Includes G. I. Taylor, 1946, (16-18).

Carstens, M. R., F. M. Neilson and H. D. Altinbilek, 1969, "Bed forms generated in the laboratory under an oscillatory flow: analytical and experimental study", U. S. Army Corps of Engineers, Coastal Eng. Res. Center, Tech Memo 28, 105 pp.

Clifton, H. E., 1976, "Wave-formed sedimentary structures--a conceptual model", SEPM Special Publication, *(in press)*.

Cooley, J. W., and J. W. Tukey, 1965, "An algorithm for the machine calculation of complex Fourier series", Mathematics of Computation, vol. 19, no. 90, p. 297-301.

Darwin, G. H., 1883, "On the formation of ripple mark in sand", Proc. Roy. Soc. London, Series A, vol. 36, p. 18-43.

Dingler, J. R., 1974, "Wave formed ripples in nearshore sands", Ph.D. thesis, University of California, San Diego, 133 pp.

Dingler, J. R., J. C. Boylls, and R. L. Lowe, 1976, "A high-frequency sonar for profiling small-scale subaqueous bedforms", unpublished manuscript.

Hunt, A. R. 1882, "On the formation of ripple-mark", Proc. Roy. Soc. London, Series A, vol. 34, p. 1-18.

Inman, D. L., 1957, "Wave-generated ripples in nearshore sands", Beach Erosion Board, U. S. Army Corps of Engineers, Tech. Memo 100, 65 pp.

Inman, D. L. 1974, Unpublished teaching notes: S10 216 Physics of Sediment Transport, University of California, San Diego, California.

Inman, D. L. and R. A. Bagnold, 1963, "Littoral processes", The Sea, vol. 3, M. N. Hill, ed., Interscience, New York, 529-553.

Inman, D. L. and A. J. Bowen, 1963, "Flume experiments on sand transport by waves and currents", Proc. Eighth Conf. Coastal Engng., Amer. Soc. Civil Eng., p. 137-150.

LeMehaute, B., D. Divoky and A. Lin, 1969, "Shallow water waves: a comparison of theories and experiments", Proc. Eleventh Conf. Coastal Engng., Amer. Soc. Civil Eng., p. 86-96.

Lowe, R. L., D. L. Inman, and B. M. Brush, 1973, "Simultaneous data system for instrumenting the shelf", Proc. Thirteenth Conf. Coastal Engng., Amer. Soc. Civil Eng., vol. 1, p. 95-112.

May, J. P., "Ability of various waterwave theories to predict maximum bottom orbital velocities in the shoaling wave zone", Coastal Research Notes, vol. 4, No. 6, p. 7-9.

Mogridge, G. R., J. W. Kamphuis, 1973, "Experiments on bed form generation by wave action", Proc Thirteenth Conf. Coastal Engng., Amer. Soc. Civil Eng., vol.2, pp. 1123-1142.

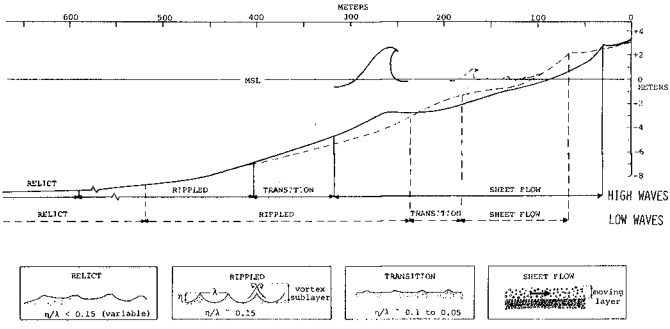

Figure 1. Range in characteristic ripples under varying wave conditions in nearshore waters (modified from Inman, 1974).

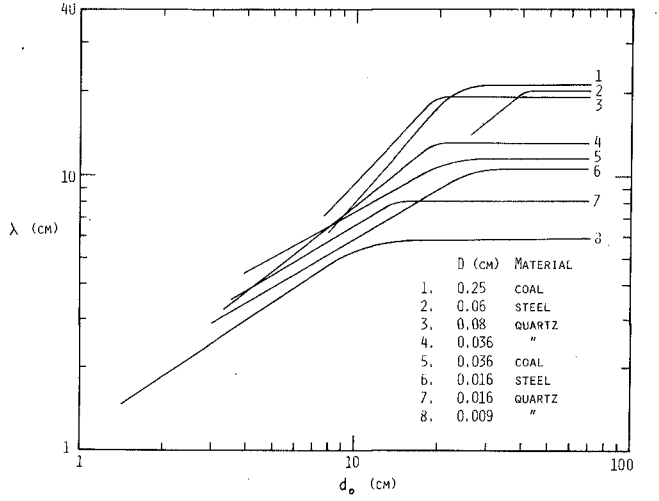

Figure 2. Relation between ripple wavelength λ and orbital diameter d_0 for sand size material of various grain sizes and densities (Bagnold, 1946).

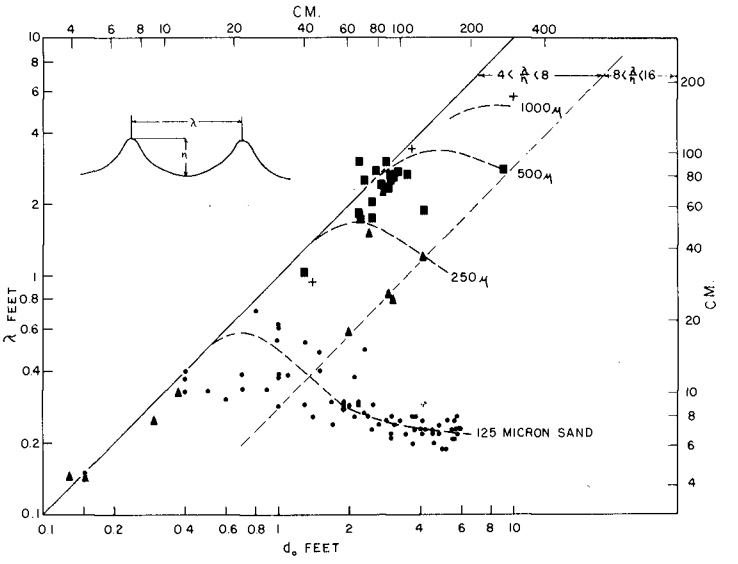

Figure 3. Dependence of ripple wavelength λ on orbital diameter d_0 for ocean waves (Inman, 1957).

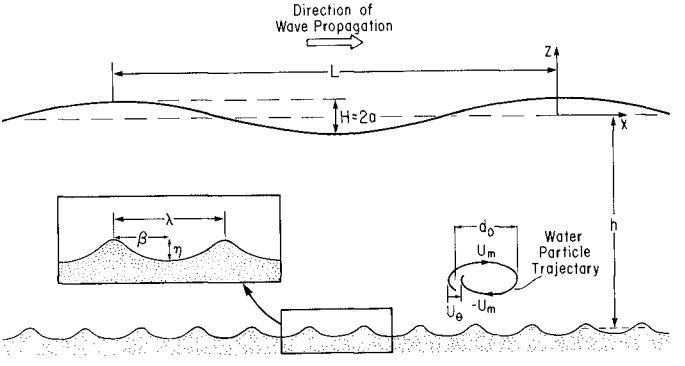

Figure 4. Definition sketch for wave and ripple parameters used in this study.

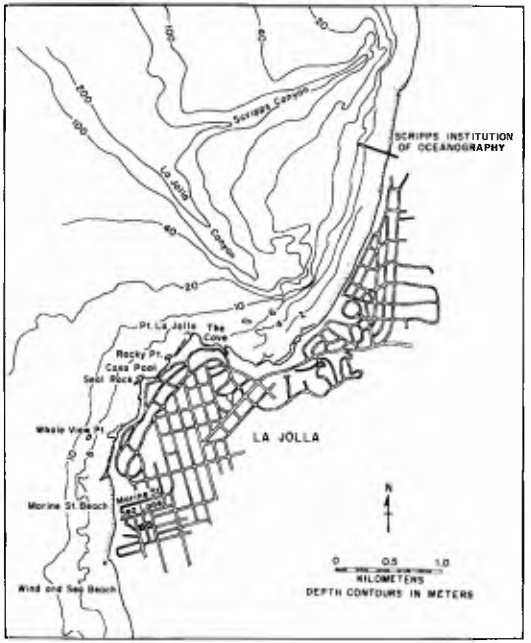

Figure 5. Location map for field sites at La Jolla, California. Experimental sites were: (1) off Scripps Institution of Oceanography pier, (2) outside Casa Pool, and (3) off Marine Street Beach at Sea Lane.

Figure 6. Fish-eye photographh of sonar transducer and mounting frame on site over a fine sand bed (Photograph by Tom Harman).

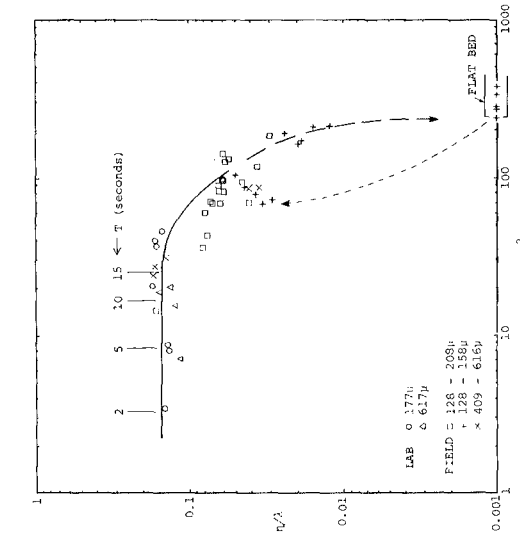

Figure 8. Ripple steepness η/λ as a function of relative stress θ with the spectral analysis wave computations □ converted to $H_{1/3}$. Symbol explanation otherwise the same. Data trends indicated by dashed lines. Short vertical lines give the onset of grain motion for selected wave periods (from Dingler, 1974).

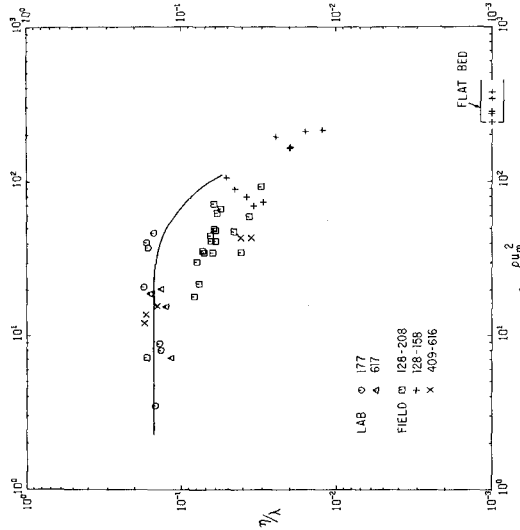

Figure 7. Ripple steepness η/λ as a function of relative stress θ. The solid line shows the mean of earlier data (Inman, 1957; Carstens, et al., 1969). All data are from the present study. Wave computations based on:
□ , spectral analysis using Hrms;
○ , △ , steady amplitude (laboratory); +, x, single wave (field).
Median diameter in microns. Values in the box on the abscissa indicate scans where the sonar profiled a flat bed.

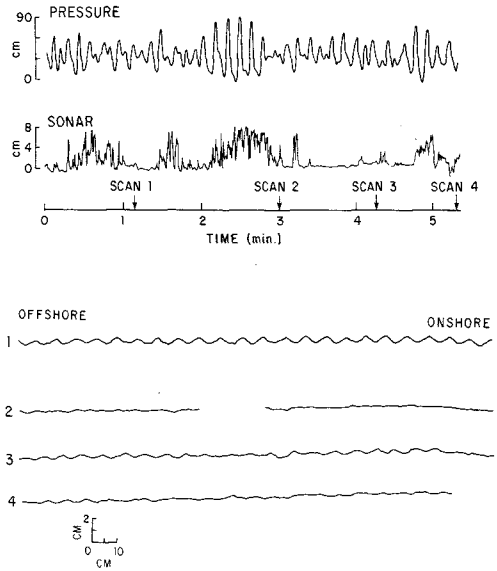

Figure 9. Analog records from field experiment of 23 October 1973 showing pressure and sonar at rest (above) and sonar scans 1-4 (below). Site north of Scripps Institution of Oceanography pier at a water depth of 3.4 meters. Bottom composed of fine sand with a median diameter of 151 μm.

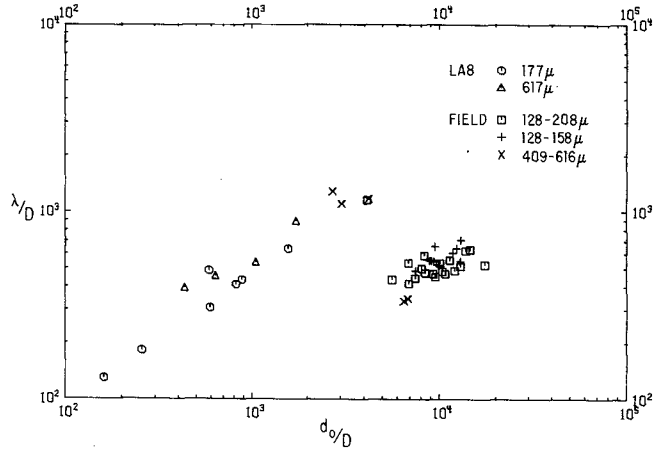

Figure 10. Dependence of relative ripple wavelength λ/D on dimensionless number d_0/D for field experiments in beds of quartz material. Data from the present study.